



Quantification of MAP and Molecular Motor Activities on Geometrically Controlled Microtubule Networks

Didier Portran, Jeremie Gaillard, Marylin Vantard,* Manuel Thery*

Laboratoire de Physiologie Cellulaire et Végétale, Institut de Recherches en Technologies et Sciences pour le Vivant, UMR5168, CNRS/CEA/INRA/Université Joseph Fourier, Grenoble, France

Received 7 August 2012; Accepted 17 September 2012

Monitoring Editor: Bruce Goode

The spatial organization of the microtubule (MT) network directs cell polarity and mitosis. It is finely regulated by hundreds of different types of microtubule-associated proteins and molecular motors whose specific functions are difficult to investigate directly in cells. Here, we have investigated their functions using geometrically controlled MT networks in vitro in cell-free assay. This was achieved by developing a new method to spatially define MT nucleation using MT microseeds adsorbed on a micropatterned glass substrate. This method could be used to control MT growth and the induction of complex MT networks. We selected the interaction of two radial arrays of dynamic and polarized MTs to analyze the formation of the central antiparallel MT bundle. We investigated the effects of the MT cross-linker anaphase spindle elongation 1 (Ase1) and the kinesin motor Klp2, which are known to regulate MT organization in the spindle midzone. We thus identified the respective roles of each protein and revealed their synergy on the establishment of stable antiparallel MT bundles by quantifying MT interactions over hundreds of comparable MT networks. © 2012 Wiley Periodicals, Inc

Key Words: microtubule, micro-patterning, MAP, Ase1, Klp2

Additional Supporting Information may be found in the online version of this article.

Ase1, anaphase spindle elongation 1; BRB80, Brinkley Buffer 80; Klp2, kinesin like protein 2; MAP, microtubule associated protein; MT, microtubules; TIRF, total internal reflexion fluorescence; SEM, standard error mean

*Address correspondence to: Laboratoire de Physiologie Cellulaire et Végétale, Institut de Recherches en Technologies et Sciences pour le Vivant, UMR5168, CNRS/CEA/INRA/Université Joseph Fourier, LPCV/iRTSV/CEA, 17 rue des Martyrs, 38054, Grenoble, France. E-mail: marylin.vantard@cea.fr or manuel.thery@cea.fr

Published online in Wiley Online Library (wileyonlinelibrary.com).

Introduction

Microtubules (MTs) are essential to all eukaryotic cells. They assemble into dynamic networks supporting many different cellular functions ranging from intracellular transport to spatiotemporal orchestration of cell mitosis. Cell physiology is, therefore, highly sensitive to MT network spatial organization. Many mechanisms have been developed and selected during evolution to ensure the precision and reproducibility of MT network architecture. MT networks can adopt a large variety of configurations from radial to linear arrays [Bartolini and Gundersen, 2006; Mimori-Kiyosue, 2011]. These architectures result from the sequential nucleation, growth, and spatial organization of MTs.

MT organization is regulated by numerous MT-associated proteins (MAPs) and molecular motors, which crosslink, regulate MT assembly/organization, and exert mechanical forces on MTs [Furuta and Toyoshima, 2008; Walczak and Shaw, 2010; Jiang and Akhmanova, 2011; Loughlin et al., 2011]. Due to the critical role of MTs in the regulation of core cell functions, there is a high degree of molecular redundancy between the multiple MAP types present in each cell [Sasabe and Machida, 2006]. It is, therefore, difficult to identify their respective contribution to network architecture and even more difficult to quantify such contributions, although several experimental approaches have attempted to address these questions.

Mitotic spindle geometry is most often used as a good readout for MT organization defects due to its reproducible and regular geometry [Walczak et al., 1998; Sharp et al., 2000; Loughlin et al., 2008]. Defective mitotic spindle conformations, such as monopolar, multipolar elongated or short spindles, led to the identification of activities associated with several MAPs and motors [reviewed in Wordeman, 2011]. The regular and reproducible shape of yeast cells in which there are only few MT bundles (three to five) also provides a good readout for MT organization compared to the 100 MTs per cell in

multicellular organisms that can adopt highly variable architectures [Tran et al., 2001; Loiodice et al., 2005].

However, in these experimental approaches, the MAP activity is indirectly inferred from the consequences of its loss. Therefore, to help draw a more specific and direct conclusion on the role of a MAP on MT organization and functioning, it is necessary to add the MAP in to a situation where it was not present, rather than to remove it. These sorts of manipulations can be performed in reconstituted *in vitro* systems. These systems are advantageous because MT networks can be created out of the minimum necessary components and thereby artificially reducing the possibility of redundancy when testing the function of a MAP.

In reconstituted systems, MTs are either free to move (in bulk solution or on surfaces) [Kapitein et al., 2005] or randomly attached to surfaces [Bieling et al., 2010; Subramanian et al., 2010; Tulin et al., 2012], therefore the spatial information that was provided by the reproducible shape of yeast or mitotic spindle architecture is lost. To get such information, it is necessary to impose controlled geometrical boundary conditions. This has been achieved by using microfabricated devices such as microwells, microgrooves, or micropatterned surfaces. The positioning of MT aster-like structures in microwells, the walls of which were coated with kinesins, revealed the contribution of pushing and pulling forces in the aster centering mechanism [Holy et al., 1997; Laan et al., 2012]. The micropatterning of DNA-coated beads, capable of inducing MT nucleation in mitotic cell extracts, can be used to study the spindle poles self-organization and focusing by molecular motors [Dinarina et al., 2009].

Here, we have developed a new method that uses micropatterned surfaces to control MT spatial nucleation and enable us to work on define MT patterns. In contrast to *in vitro* experiments studying the self-organization of free MTs [Nedelec et al., 1997; Surrey et al., 2001], our goal was to investigate how MAPs and molecular motor regulate MT organization when they encounter at specific orientations predetermined by geometrical boundary conditions. With this technique, we were able to induce the formation of more or less complex but controlled MT network geometries in which dynamic MTs could exist as single entities or as parallel or antiparallel bundles. In validating the MT networks created by this method, we chose aster-like structures to compare the specific contributions of anaphase spindle elongation 1 (Ase1; the yeast ortholog of human PRC1, *Drosophila* Feo and plant MAP65-1), which has been shown to be involved in antiparallel MT alignment and spindle formation [Loiodice et al., 2005; Janson et al., 2007; Bieling et al., 2010; Tulin et al., 2012], and of kinesin like protein 2 (Klp2; member of the kinesin 14 family, yeast ortholog of human HSET, *Drosophila* Ncd, and plant ATK5), which has been shown to be involved in parallel MT stabilization, antiparallel

MT sliding, and spindle length control [Carazo-Salas et al., 2005; Janson et al., 2007; Braun et al., 2009; Fink et al., 2009].

Results

Micropatterning of MT Seeds

The MT interaction assay we have developed is based on the growth of MTs out of micropatterned nucleation sites. It requires the specific attachment of MT nucleation templates onto micropatterned sites and their elongation in the presence of purified tubulin dimers. MT nucleation templates consisted of short (0.5 μm on average) stabilized MTs (later referred to as MT seeds) obtained by polymerizing both Alexa561-labelled and biotinylated tubulin at 50 μM , in the presence of GMPCPP and taxol at 37°C (Supporting Information Fig. S1). To prevent the nonspecific adsorption of these MT seeds on the substrate, the glass coverslip was cleaned, oxidized, and then treated with a silane functionalized with Poly-Ethylene-glycol (PEG) chains (step 1–2 in Fig. 1A). The dried PEG-coated slide was placed into contact with a photomask, on which the micropatterns of interest were transparent and exposed to deep UV light (wavelength below 200 nm) (step 3 in Fig. 1A). Deep UVs induced the oxidation of the exposed regions making these regions competent to absorb protein [Azioune et al., 2009]. The micropatterned slide was then mounted in a flow chamber, in which a solution of neutravidin was added (step 4 in Fig. 1A). To prevent the nonspecific adsorption of MAPs, the micropatterned coverslip was further incubated with poly-lysine-PEG to improve substrate passivation (step 5 in Fig. 1A). Biotinylated MT seeds were then introduced in the chamber in a solution that flowed over the micropattern to ensure specific linkage to neutravidin on the micropatterns and further elongated by the addition of Alexa488-labelled tubulin in presence of GTP (step 6–7 in Fig. 1A). Depending on the choice of micropattern, we could induce MT growth out of any kind of nucleation geometries such as dots, curved, or straight bars (Fig. 1B, movie S1).

Controlled MT Orientation

MT orientations appeared to depend on the geometry of the nucleation region. Their growth was observed in real-time using dual-view total internal reflection fluorescence (TIRF) microscopy under temperature-controlled conditions at 32°C. When nucleated from a bar micropattern, most MTs had a biased orientation orthogonal to the longitudinal axis of the bar (Fig. 2A). In contrast, MTs appeared radially oriented and randomly distributed through 360° when nucleated from a dot-shaped micropattern (Fig. 2B).

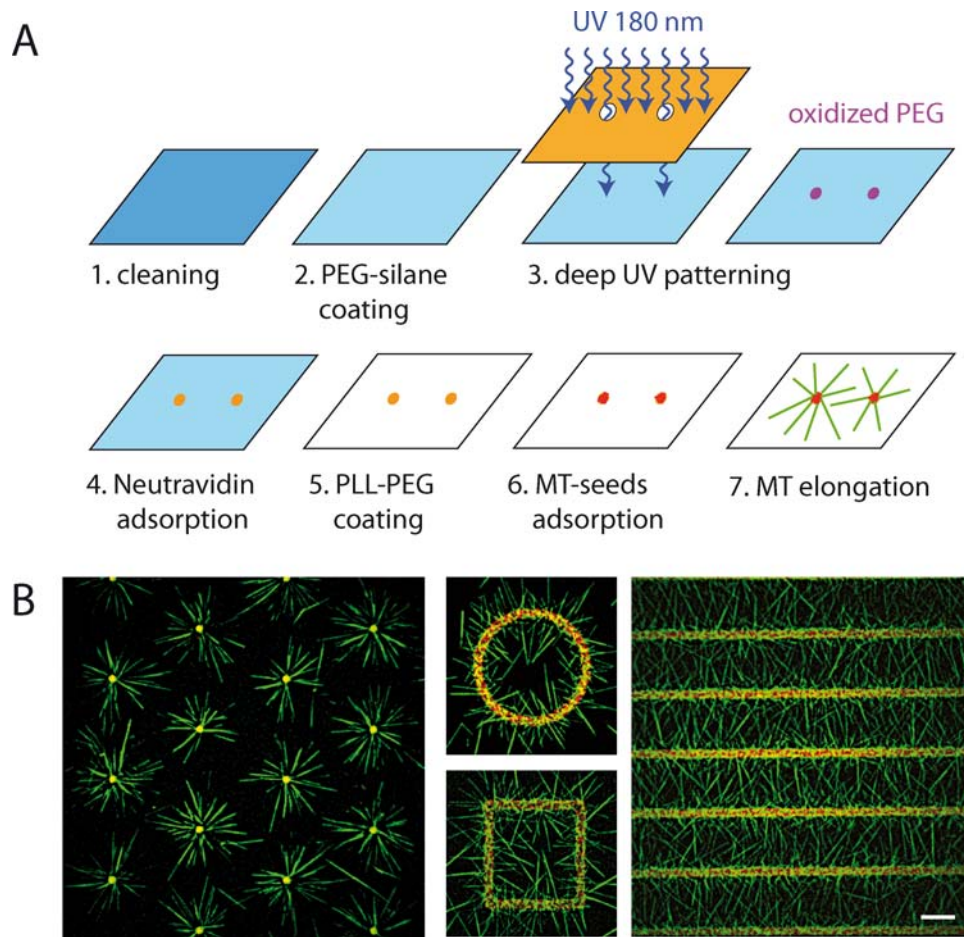


Fig. 1. Geometrical control of MT growth. (A) Schematic representation of the micropatterning protocol. (B) MT (green) growth out of dots and lines coated with microseeds (red). MTs are revealed by ATTO-488 tubulin and microseeds by ATTO-565 tubulin. Scale bar is 10 μ m.

MT orientations could be controlled by using longer MT seeds (2–5 microns). In this case, fluid flow appeared to align MT seeds, which were no longer evenly oriented on the micropattern surfaces. In these conditions, MT growth from a dot-shaped or a bar-shaped micropattern was biased along the direction of the flow during MT seed adsorption (Supporting Information Fig. S2).

Controlled MT Polarity

The direction of MT polarity could be inferred from the measurement of growth speed since minus-ends grow at lower rates than plus ends [Walker et al., 1988]. Distributions of growth speeds revealed that, regardless of the geometry of the nucleation region, a mean of 80% [standard error men (SEM), 3%] of MTs had their minus-end on the micropattern and their plus end positioned away from it (Fig. 2C). Therefore, nucleation from short MT seeds on dots appeared to mimic the radial organization of aster-like structures (and subsequently referred to as asters) with minus-ends at the center and plus ends at the periphery.

Imaging of MAP-Induced MT Organization in Real Time

Isotropic and polarized growth of MTs from dots allowed us to induce controlled antiparallel MT interactions at various angles between two asters (Fig. 3A). These interactions between asters were selected to test the specific role of a MAP, Ase1, and a molecular motor Klp2. Full-length recombinant His-Ase1 was purified from *E. coli* (Supporting Information Fig. S3A) that have an apparent K_d of 41 ± 7 nM (Supporting Information Fig. S3C) and functionally tested by MT bundling assays (Supporting Information Fig. S3B). Full-length recombinant SNAP-Klp2-His was purified from *E. coli* (Supporting Information Fig. S3A), (apparent K_d 72 ± 5.8 nM, Supporting Information Fig. S3D). Its functionality was tested by ATPase assays in presence of MTs (Supporting Information Fig. S3E) and by its ability to slide MTs (Supporting Information Fig. S3F). Real-time monitoring of MT behaviors showed that in presence of either MAP, MT interactions between two asters could lead to MT reorientation and/or stabilization. In the absence of either MAP, antiparallel MT interactions appeared capable of only inducing transient MT reorientation and antiparallel alignment (Fig. 3B and Supporting

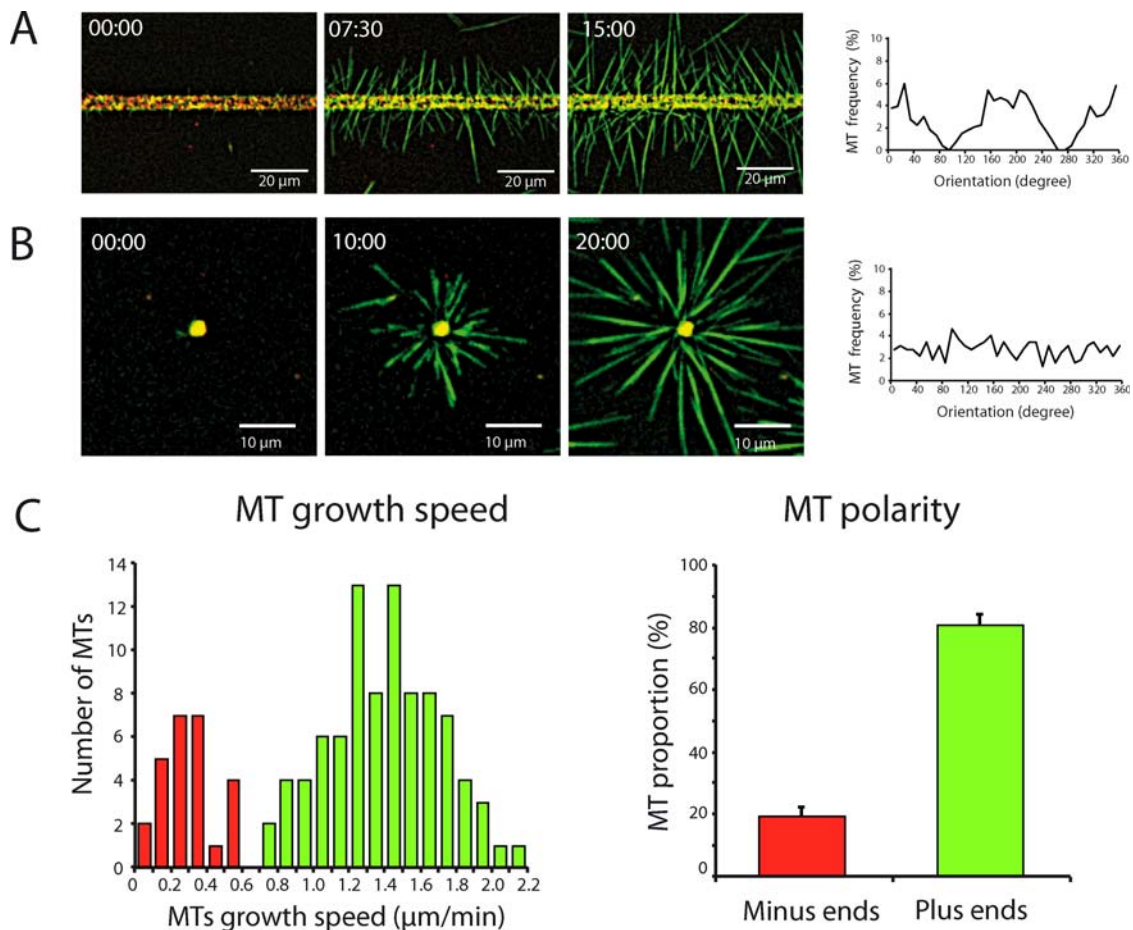


Fig. 2. Control of MT orientation and polarity. (A, B) Real time monitoring of MT growth out of a 3-micron-wide bar (A) and a 3-micron-wide dot (B). Angular distribution of MTs is represented by the proportion of MTs in every 10° wide angular sectors. On the bar micropattern, MT orientations appeared biased orthogonally to the longitudinal axis of the bar (A); and on the dot micropattern, orientations were radial and appeared evenly distributed through 360° (B). Distribution of MT growth speed (left) displayed two separated Gaussian populations corresponding to the minus-ends growth speed from 0 to 0.7 $\mu\text{m}/\text{min}$ (red) and the plus end growth speed from 0.8 to 2.2 $\mu\text{m}/\text{min}$ (green). (C) The relative proportions of MT plus-ends and minus-ends (right) are calculated from this distribution (mean \pm SEM).

Information movie S2). In the presence of Klp2, antiparallel MTs have been observed to coalign (Fig. 3C and Supporting Information movie S3). However, MT depolymerization or detachment from the micropattern by sliding led to the dismantling of antiparallel bundles after a few minutes (Fig. 3C and 3D and Supporting Information movies S3 and S4). In the presence of Ase1, antiparallel bundles could also form between two asters and these bundles seemed to persist for longer periods than with Klp2 (Fig. 3E and Supporting Information movie S5). In the presence of both Ase1 and Klp2, antiparallel MTs with large angular deviations (40° in Fig. 3F compared with 22° for Ase1 alone in Fig. 3E) could be reoriented and stabilized (Fig. 3F and Supporting Information movie S6).

Identification of Stable MAP-Induced MT Organization

To identify the steady organizations of the MT spindle like array with those MAPs, snapshot of patterns in these

different conditions were taken after 30 min of polymerization (Fig. 4). Because the positions of the two nucleation sites of the asters were defined by the micropattern, these positions also defined the two reference points for overlaying images to create an overall average image. MT fluorescence intensities were normalized such as single MTs had the same fluorescence intensity in all conditions. Averaged image provided an intensity distribution of the MTs around the two asters and revealed local accumulation of MTs in response to MAPs (Fig. 4A). The visual information provided by the color-coding of these averaged distributions (Fig. 4B) could be turned into a quantitative measure by performing a linescan along the midline separating the two asters (Fig. 4C). This analysis confirmed that Klp2 alone had limited effect on durable MT accumulation along the central axis connecting the two asters. Strikingly, Ase1 induced a broad MT accumulation at the central axis. This showed that Ase1 has limited reorientation capacities since antiparallel bundles could not completely align with the central axis, probably due

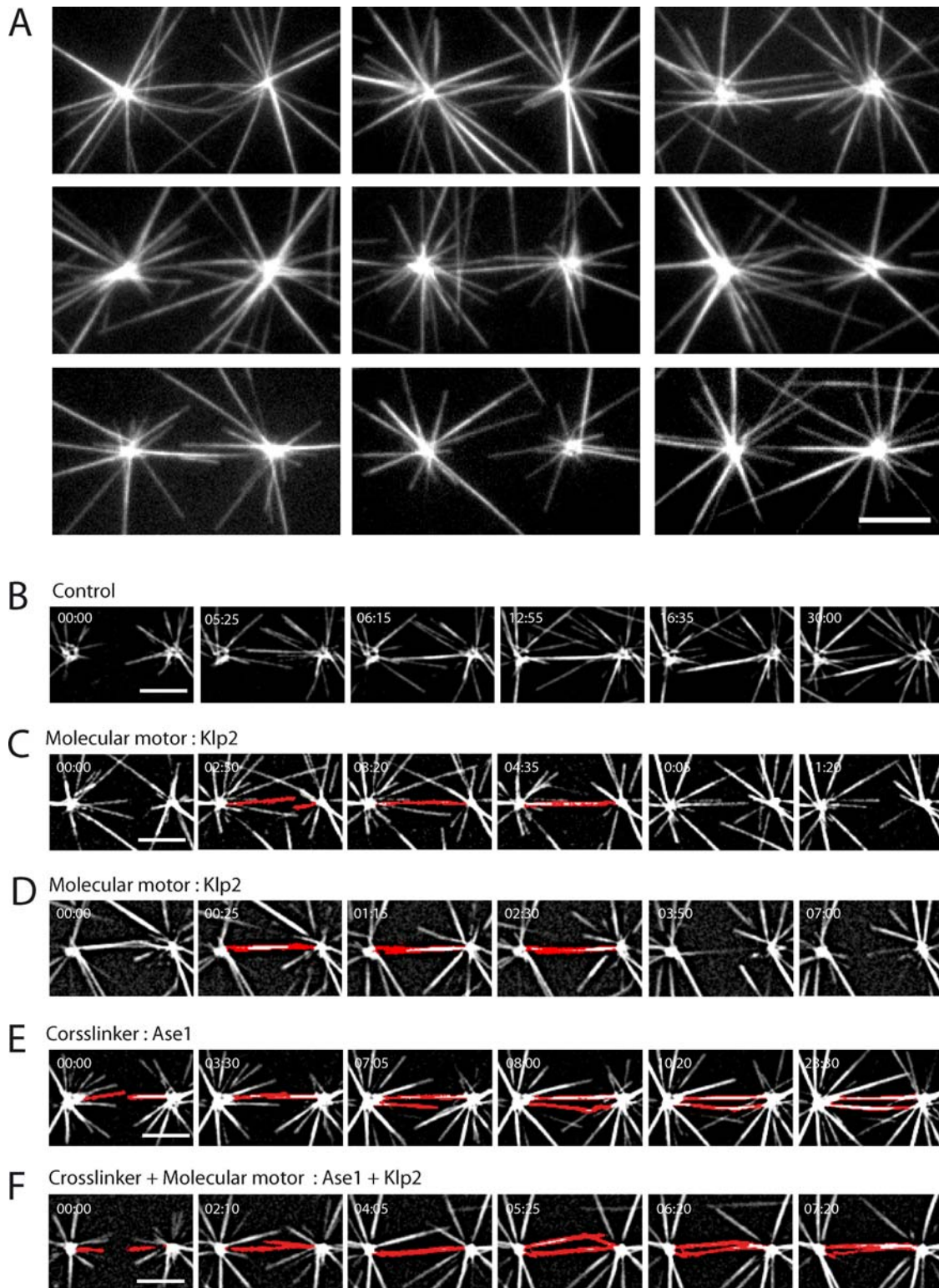


Fig. 3. Dynamic regulation of antiparallel MT bundle formation by Ase1 and Klp2. (A) Representative images showing nine distinct pairs of aster-like structures in the absence of MAPs. MTs were revealed by ATTO-488 tubulin. (B–F) Time lapse imaging in TIRF microscopy of MT interaction in the absence of MAPs (B), in the presence of 5 nM of Klp2 (C–D), 33 nM of Ase1 (E) or both (F). MTs forming antiparallel bundles are highlighted in red. Scale bars represent 10 μm .

to the crosslinking effect preventing MT sliding. Interestingly, Klp2 appeared capable of affecting this distribution of MTs because in response to the cooperation of Klp2

and Ase1, MTs accumulated along the central axis between the two nucleation sites with a much sharper angular distribution (Figs. 4B and 4C).

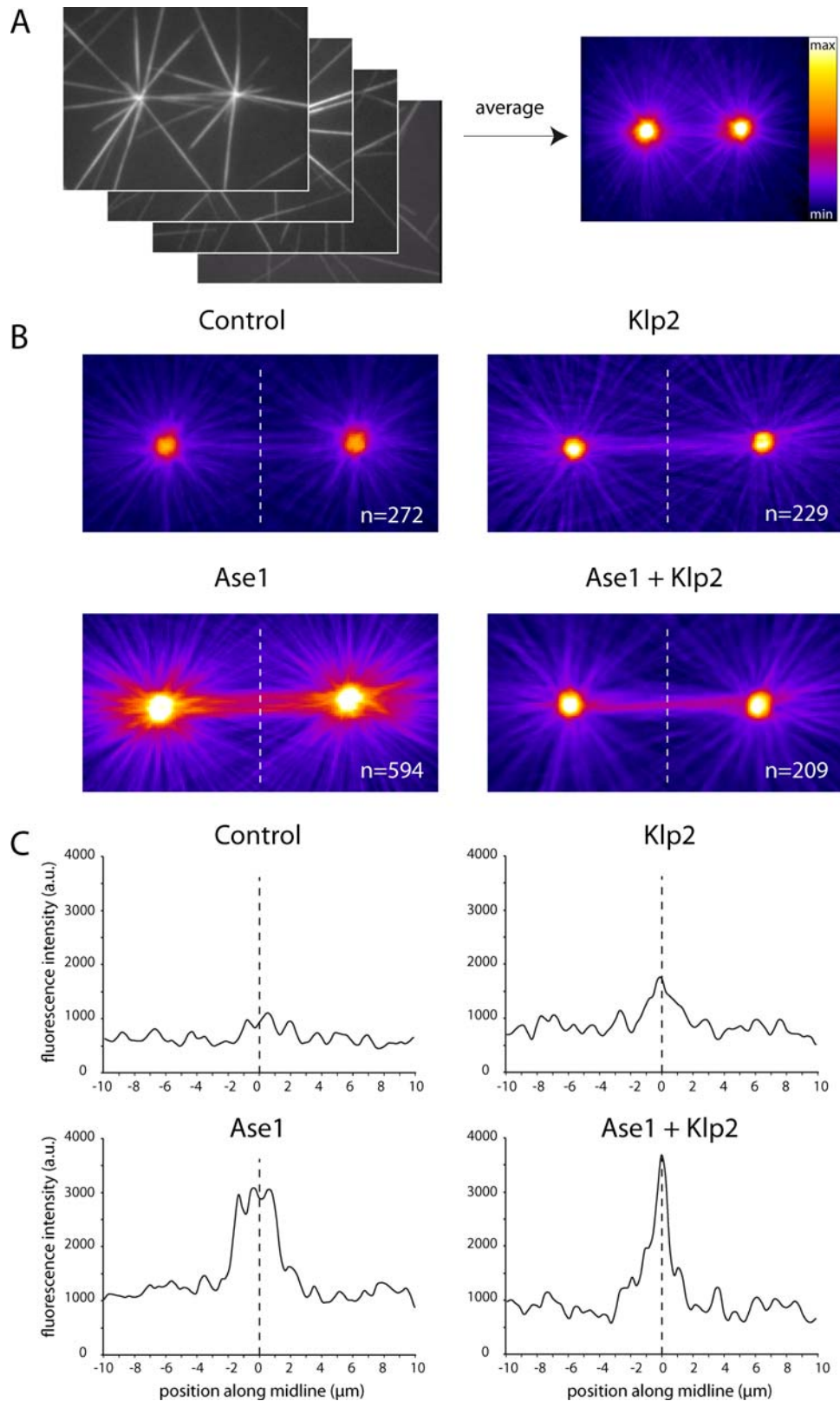


Fig. 4. Quantification of antiparallel MT bundle formation by Ase1 and Klp2. (A) Images of MTs, revealed by ATTO-488 tubulin, were taken after 30 min of polymerization, then overlaid and averaged. Averaged image color-coding (“FIRE” look-up table) reveals the most frequent structures in orange/yellow (right). (B) Averaged images were obtained in the control condition (without MAPs), in presence of 33 nM of Ase1, in presence of 5 nM of Klp2 and in presence of both. (C) Linescans of fluorescence intensity along the midline separating the two asters. Fluorescence peaks revealed the formation of a broad distribution of stable bundles by Ase1 and a sharper distribution of aligned bundles by the combination of Ase1 and Klp2.

Therefore, we conclude that Ase1 is capable of aligning and slightly reorienting antiparallel MTs. However, its crosslinking activity inhibits MT sliding and more substantial MT reorientation. Klp2 is capable of reorienting and sliding antiparallel MTs along each other but does not support the formation of stable crosslinks. Therefore, Ase1 and Klp2 appear to have a synergistic effect on MT bundle formation in which Klp2 reorients and aligns antiparallel MTs while Ase1 crosslinks and maintains them in a steady-state (Fig. 5).

Asters Separation Modulates Antiparallel Bundle Formation

We next tested whether the distance between two MT asters could affect the antiparallel MT organization by comparing bundle formation between asters separated by 15 and 30 μm . We measured the MT bundles accumulation in presence or in absence of Ase1. In control conditions, that is, in the absence of MAP, antiparallel MT bundles could form only in short spindle-like structures (Figs. 5A and 5B). In presence of Ase1, antiparallel bundles could form on long and short spindle-like structures but the bundling region appeared wider on the short ones (Figs. 5A and 5B). To test whether this higher number of antiparallel MT bundles in short spindles resulted from increased MT densities in the overlapping regions or from variations in Ase1 bundling efficiency, we normalized the Ase1-induced fluorescence signal along the linescan to the fluorescence measured in control conditions. The angular variations of the normalized fluorescence signal were quite similar in short and long spindles (Fig. 5C). This suggested that Ase1 efficiency was identical in both conditions and that the increase of MT bundles in short spindles resulted from more frequent MT overlaps. Indeed, it is quite intuitive that, for a given concentration of free tubulin, and thus for a given MT length distribution, variations in spindle length modulate the local density of MT overlap in between the asters and thus the number of antiparallel MT bundles.

Discussion

We have developed a new method to direct dynamic MT self-organization into controlled network geometries. This has been achieved by improving previous surface micropatterning protocols for *in vitro* assays [Reymann et al., 2010] through precisely defining the location of MT nucleation sites, preventing the nonspecific adsorptions of tubulin and MAPs and developing efficient MT nucleation seeds.

The grafting of MT microseeds onto micropatterns significantly improved the nucleation efficiency compared with using microcontact printed centrosome fragments [Shang et al., 2009] or micropatterned gamma-tubulin

[Yang et al., 2006]. In addition, MT nucleation from short seeds appeared to play a key role in the polarized organization of aster-like arrays. Short seeds were densely packed and randomly oriented on the micropatterns. MT plus-ends grew more rapidly than minus-ends ($1.7 \pm 0.2 \mu\text{m}/\text{min}$ versus $0.4 \pm 0.1 \mu\text{m}/\text{min}$). Thus, they could more efficiently escape from the micropattern without being perturbed by the local steric constraints. This could account for the presence of a large majority ($80 \pm 3\%$) of MT plus-ends growing out of the micropattern. MTs polymerized from long MT seeds (2–5 μm) appeared less reproducibly polarized (60% of MT plus-ends out of the micropattern). This could be explained by the fact that longer seeds were less densely packed, allowing the unconstrained growth of both rapid plus-ends and slow minus-ends.

The double surface passivation with silane-PEG and PLL-PEG offers unprecedented repellent properties and therefore preserves the unconstrained growth of MTs out of the micropatterned sites compared to glass [Shang et al., 2009], silica [Yang et al., 2006]. Hence, the highly controlled surface and biochemical conditions enable MTs to assemble into predictable and reproducible dynamic networks.

Surface micropatterning has greatly contributed to the identification of the morphogenetic rules guiding intracellular as well as multicellular organizations [Théry, 2010]. This method, when applied to cell-free biomimetic approaches, has revealed the critical role of actin filament nucleation geometry in the regulation of network architecture and the development of mechanical forces [Reymann et al., 2010, 2012]. Our method now paves the way for the quantitative description of the morphogenetic rules governing the MT network architecture and dynamics.

In this study, we selected the aster-pair arrangements to examine the interaction of MTs with opposed polarities in the presence of MAPs and molecular motors. One of the key features of this assay is that it is based on dynamic MTs. Our analysis of averaged asters interactions showed that no stable antiparallel MT bundles or specific organization can be formed in the absence of Ase1 or Klp2. In the presence of Klp2, antiparallel MTs can reorient and align MTs but this overlap is short-lived since MTs can slide and separate or depolymerize. It seems relevant to take into account this last phenomenon when considering MT network organization *in vivo* because MT assembly and disassembly would also modulate the actual contribution of a MAP to the eventual network architecture. Our results also suggest that Ase1 may reduce the depolymerization rate of MTs in antiparallel bundles. The stabilization of MTs inside a bundle organized by MAP65s has not yet been well defined. However, *in vivo* and *in vitro* studies have shown that MTs bundled by MAP65-1, Ase1 homolog in plants, are resistant to depolymerization [Van Damme et al., 2004; Li et al., 2007; Meng et al., 2010].

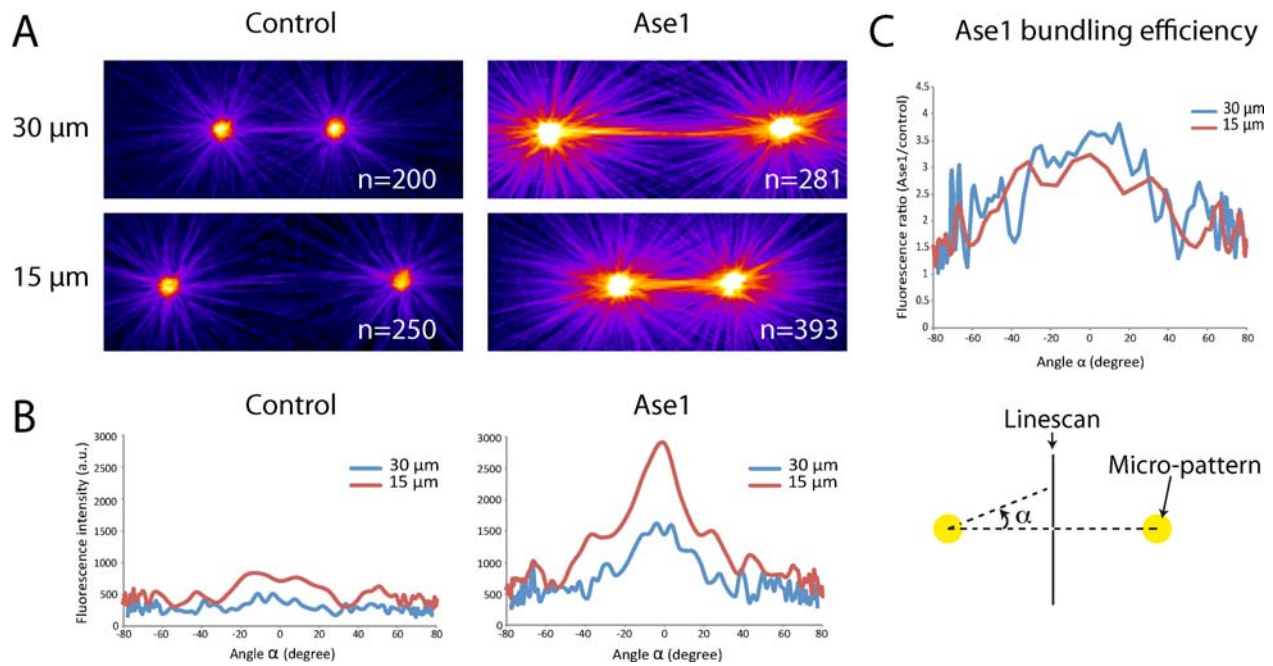


Fig. 5. Distance between asters regulates the number of antiparallel MT bundles. (A) Averaged images were obtained in control conditions (without MAPs) and in presence of 33 nM of Ase1 for two different distances between disk micropatterns: 15 and 30 μm. Averaged image color-coding (“FIRE” look-up table) revealed the most frequent structures in orange/yellow (right). (B) Angular distributions of fluorescence intensity along the midline separating the two asters. The scheme on the right represents the linescan and the angle measure. Fluorescence peaks revealed that more bundles are formed as the asters become closer, and that Ase1 favors their assembly in both conditions. (C) Ase1 fluorescence signal along the linescan normalized with the signal in control conditions. The plot shows no differences in the angular variations of Ase1 bundling efficiency between short and long spindles.

A recent study has also shown that MT bundles organized by MAP65-4, (belonging to the MAP65 family in *Arabidopsis thaliana*) have a rescue factor activity by acting as a brake to depolymerization [Fache et al., 2010]. Furthermore, the crosslinking activity of Ase1 [Janson et al., 2007] presumably prevented Klp2-induced MT separation after sliding [Braun et al., 2011] and can explain why the synergy between Klp2 and Ase1 was necessary in the formation of stable antiparallel bundles.

In this system, we could also modulate the geometrical configurations of spindle-like structures and reveal the effect of spatial boundary conditions on the formation of antiparallel MT bundles. It clearly appeared that variations of MT densities in response to asters separation do not affect Ase1 bundling efficiency and that the number of overlapping MTs directly impacts the final number of bundles.

The controlled and reproducible geometry of the MT networks allowed the detection of subtle architectural changes by comparing the network geometry at steady state to a standard reference without MAPs. The observation of many similar asters at a given time point indirectly revealed the fluctuations of the organization process. Our method is also fully compatible with high quality time-lapse imaging, which we used to characterize the transient MT organization like MT sliding induced

by Klp2. The low density of MTs and high quality images from TIRF microscopy enabled the tracking of single MTs or MT bundles. Therefore the automatic acquisition and analysis of thousands of aster pictures or time-lapse “on chip” should provide the necessary amount of data to detect significant changes in MT dynamics and organization.

In conclusion, this new method permits the formation of complex but reproducible MT network geometries, made of multiple MTs with controlled polarities. In addition to quantifying the role of MAPs, micropattern-defined MT nucleation sites can also be used to study MT network self-organization in response to geometrical constraints and should prove useful in the investigation of the complex mechanisms underlying intracellular organization.

Materials and Methods

Tubulin Purification

Tubulin was purified from fresh bovine brain by three cycles of temperature-dependent assembly/disassembly according to Shelanski [1973] in Brinkley Buffer 80 (BRB80 buffer; BRB buffer: 80 mM PIPES, pH 6.8, 1 mM EGTA, and 1 mM MgCl₂ plus 1 mM GTP). MAP-

free neurotubulin was purified by cation-exchange chromatography (EMD SO, 650 M, Merck) in 100 mM MES, pH 6.8, supplemented with 1 mM MgCl₂, and 1 mM EGTA as described previously [Malekzadeh-Hemmat et al., 1993]. Purified tubulin was obtained after a cycle of polymerization and depolymerization.

Tubulin Labeling

Fluorescent tubulin (ATTO-488-labeled tubulin and ATTO-565-labeled tubulin) and biotinylated tubulin were prepared according to Hyman et al. [1991]. MTs from neurotubulin were polymerized at 37°C for 30 min and layered onto cushions of 0.1 M NaHEPES, pH 8.6, 1 mM MgCl₂, 1 mM EGTA, 60% volume/volume (v/v) glycerol, and sedimented by high centrifugation at 30°C. Then MTs were resuspended in 0.1 M NaHEPES, pH 8.6, 1 mM MgCl₂, 1 mM EGTA, 40% (v/v) glycerol and labeled by adding 1/10 volume 100 mM NHS-ATTO (ATTO Tec) or NHS-Biotin (Pierce) for 10 min at 37°C. The labeling reaction was stopped using 2 volumes of 2X BRB80, containing 100 mM potassium glutamate and 40% (v/v) glycerol, and then MTs were sedimented onto cushions of BRB80 supplemented with 60% glycerol. MTs were resuspended in BRB80, and a second cycle of polymerization and depolymerization was performed before use.

Ase1 Expression and Purification

Recombinant His-Ase1 and His-Ase1-GFP were expressed and purified according to Janson et al. [Janson et al., 2007]. Bacterial expression vectors pPT184 encoding His-Ase1 or His-Ase1-GFP (kindly provided by Dr. M Janson) were transfected into Rosetta2®(DE3)pLysS *E. coli* (VWR). Proteins expression was induced by 6 h incubation with 0.5 mM IPTG at 25°C. Soluble proteins were extracted from a 1:1 culture in lysis buffer (NaH₂PO₄ 25mM, NaCl 300 mM, imidazole 30 mM, lysozyme 0.1 mg/mL, DNase1 20 µg/mL, NP-40 1%; pH 7.4) using probe-tip sonicator. Lysate was added to Ni sepharose HP beads (GE), which were washed (NaH₂PO₄ 25mM, NaCl 300 mM, imidazole 30 mM; pH7.4) followed by elution (NaH₂PO₄ 25 mM, NaCl 300 mM, imidazole 250 mM; pH7.4) and dialysis over night in buffer (NaH₂PO₄ 25 mM, NaCl 300 mM; pH7.4).

To determine the K_d of Ase1, 50 nM of recombinant His-Ase1-GFP were mixed with various concentrations of taxol stabilized MTs (ranging from 0 to 1000 nM) in NaH₂PO₄ 25 mM, NaCl 100 mM, pH 7.4 and incubated for 30 min at room temperature. Samples were then centrifuged during 20 min at 100,000 *g* at 25°C. Supernatants were kept and pellets were resuspended in NaH₂PO₄ 25 mM, NaCl 500 mM, pH 7.4. The amount of His-Ase1-GFP in the pellets and supernatants was determined by spectrofluorimetry. All tubes were silanized

to limit nonspecific adsorption of proteins [Sambrook et al., 1989]. The K_d of Ase1 was determined as 41 ± 7 nM (Supporting Information Fig. S3C).

Klp2 Expression and Purification

Full-length Klp2 cDNA (gratefully provided by Dr. S Diez) was cloned into the pET-30a(+) expression vector (Novagen) with Snap Tag to N-Ter and His Tag to C-Ter. The recombinant N-terminal SNAP tagged and C-terminal His Tagged fusion proteins were transfected into Rosetta2®(DE3)-pLysS *E. coli* (VWR) and expression was induced with 0.1 mM IPTG for 16 h at 15°C. Harvested cells were resuspended in buffer A (50 mM sodium phosphate buffer pH 7.4, 2 mM MgCl₂, 1 mM DTT, 0.1 mM ATP) containing 200 mM NaCl and protease inhibitors (Roche) and lysed in 0.05% v/v Triton X-100 (Sigma) by sonification. The lysates were centrifuged 30 min at 25000 *g* and 4°C. The clear lysates were loaded onto a NiSepharose HP column (GE Healthcare). The column was washed with buffer A containing 100 mM NaCl and 20 mM imidazole. Proteins were eluted in buffer A containing 100 mM NaCl and 250 mM imidazole then desalted into buffer A containing 100 mM NaCl without ATP, and snap-frozen in liquid nitrogen.

The K_d of recombinant SNAP-klp2-His was determined as described for Ase1, except that 40 nM of Klp2 labeled with ATTO-565 was mixed with various concentrations of taxol stabilized MTs (ranging from 0 to 1500 nM) in buffer A containing 50 mM NaCl and supplemented with 1 mM AMPPNP (Jena Biosciences). The K_d of Klp2 was determined as 72 ± 5.8 nM (Supporting Information Fig. S3D).

ATPase Assay

ATPase assays were performed using a continuous coupled assay with ATP regeneration according to Hackney and Jiang (2001). Reactions (200 µL) were performed at room temperature in ATPase buffer (25 mM ACES (pH 6.9)/2 mM magnesium acetate/2 mM potassium-EGTA/0.1 mM potassium-EDTA/1 mM 2-mercaptoethanol/1 mM ATP/2 mM phosphoenolpyruvate/0.25 mM NADH/5 µg/mL pyruvate kinase/3 µg/mL lactate dehydrogenase) and started by the addition of Klp2 (50 to 250 nM). ATPase activity of Klp2 was enhanced in the presence of taxol stabilized MTs (2.5 µM). In this assay, the V_{max} of the ATPase activity was 1.1 s^{-1} in the presence of MTs (Supporting Information Fig. S3E).

Surface Micropatterning

Glass coverslips were cleaned by successive chemical treatments: 30 min in acetone, 15 min in ethanol (96.5°), rinsing in ultrapure water, 2 h in Hellmanex III (2% in water, Hellma), and rinsing in ultrapure water. Coverslips

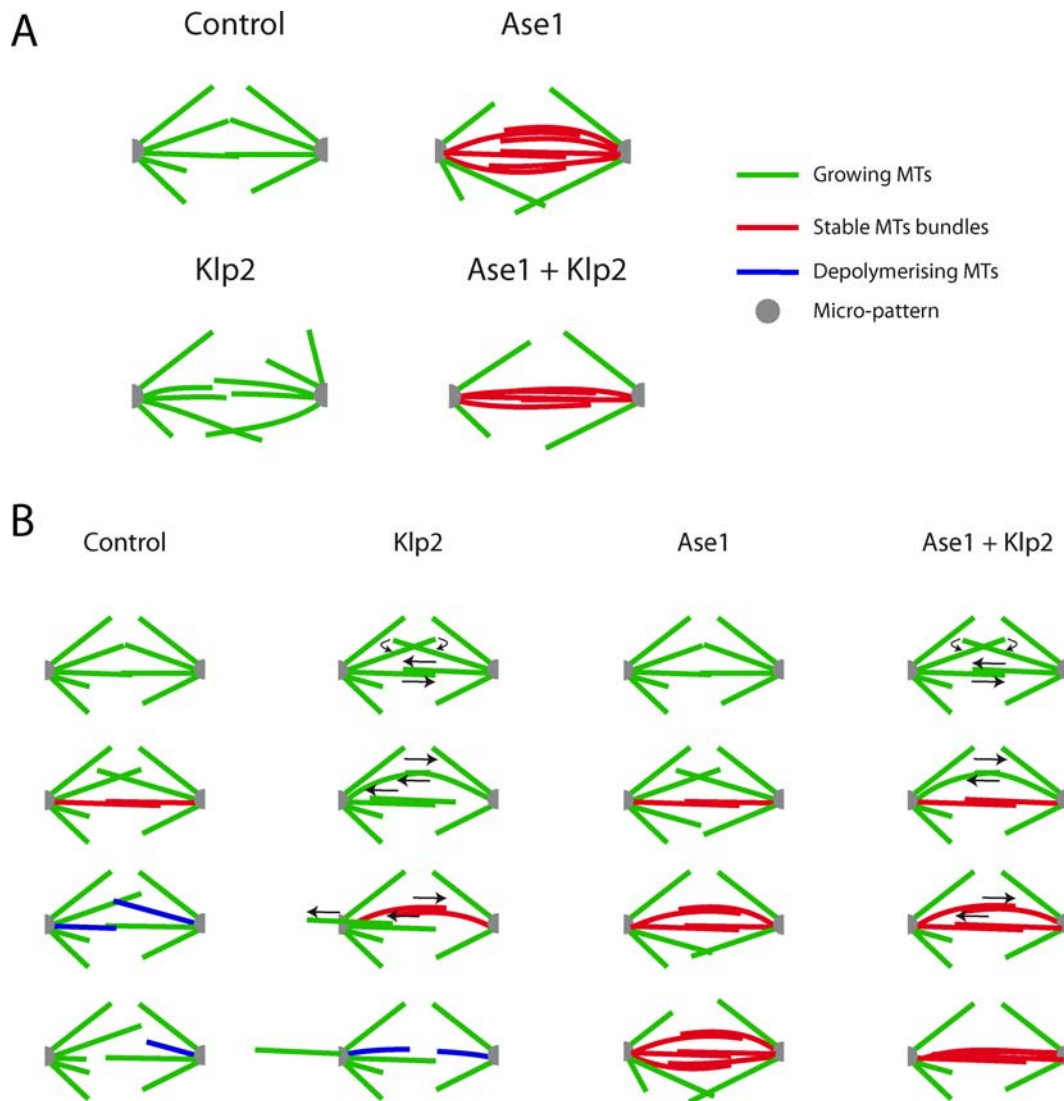


Fig. 6. Ase1 and Klp2 contribution to antiparallel bundle formation. (A) Schematic representation of antiparallel bundle formation without MAPs (control), with a crosslinker (Ase1), with a molecular motor (Klp2), and with both. In control conditions, MTs can coalign to form an antiparallel bundle but they rapidly depolymerize and disappear. (B) In the presence of Klp2, MTs are aligned along the central axis connecting the two nucleation regions but these antiparallel bundles eventually depolymerize or detach from one pole before being transported to the opposite pole. In presence of Ase1, antiparallel MT bundles are crosslinked and therefore protected from depolymerization in a wide angular sector. In the presence of both Ase1 and Klp2, MTs are aligned and then form stable antiparallel bundles along the central axis.

were then dried, filtered airflow, and oxidized in a plasma cleaner (FEMTO; Diener Electronics) during 2 min at 60 mW. Coverslips incubated overnight in a solution of triethoxy-silane-PEG (30 KDa, PSB-2014, creative PEG work) 1 mg/mL in ethanol 96.5° and 0.02% of HCl, with gentle agitation at room temperature. Coverslips were then successively washed in ethanol and ultrapure water, dried with filtered air, and store at 4°C away from dust. Passivated coverslips were placed into contact with a photomask (Toppan) with a custom-made vacuum-compatible holder and exposed to deep UV (7 mW/cm² at 184 nm, Jelight) for 30 s. Deep UV exposure through the transparent micropatterns on the photomask created oxi-

dized micropatterned regions on the PEG coated coverslip [Azioune et al., 2010].

Micropatterned MT Growth

A flow cell chamber with an approximate volume of 30 μ L was constructed with double-sided tape (70 μ m height) between a micropatterned and a passivated coverslips. The perfusion chamber was flowed with neutravidin (25 μ g/mL in BRB80; Pierce), then passivated for 1 min with PLL-g-PEG (Pll 20K-G35-PEG2K, Jenkem Technology) at 0.1 mg/mL in 10 mM Hepes (pH = 7.4) and further washed with 300 μ L of BRB80.

MT microseeds were polymerized using 50 μM of tubulin (85% of biotinylated tubulin and 15% of ATTO-565-labelled tubulin) in presence of 0.5 mM of GMPCPP and 20 μM of Taxotere in BRB80 at 37°C for 10 min. Microseed length and structure were controlled by negative-stain electron microscopy observations. Microseeds were stained on grids with 2% (w/v) uranyl acetate and observed on a CM12 microscope (FEI Eindhoven) operating at 120 kV.

MT microseeds were flowed into the chamber at 1 μM , the flow was stopped for 5 min and then the chamber was thoroughly washed. MT seeds were elongated with a mix containing 15 μM of tubulin (30% ATTO-488-labelled tubulin and 70% unlabeled tubulin) in BRB80 supplemented with 50 nM NaCl, 50 NaPi, 1 mM of GTP, an oxygen scavenger cocktail (2 mg/mL glucose, 80 $\mu\text{g}/\text{mL}$ catalase, and 0.67 mg/mL glucose oxidase), 1% BSA, 0.025% of methyl cellulose (1500 CP, from Sigma) and with or without MAPs. Ase1 and Klp2 were, respectively, used at a concentration of 33 and 5 nM.

Imaging

MT dynamics were visualized using an objective-based azimuthal ilas2 TIRF microscope (Nikon eclipse Ti, modified by Roper scientific) and Evolve 512 camera (Photometrics). Microscope stage was kept at 32°C using a warm stage controller (LINKAM MC60). Excitation was achieved using 491 and 561 nm lasers (Optical Insights). Time-lapse recording (one frame every 5 s) was performed for 30 min using Metamorph[®] software (version.7.7.5, Universal Imaging). Movies were processed to improve signal/noise ratio (equalize light, low pass and flatten background filters of Metamorph software).

Acknowledgments

The authors thank Phong Tran for critical reading of the manuscript, Emmanuelle Neuman for assistance in electronic microscopy, as well as Andrei Popov and Isabelle Arnal for providing XMAP215 and H2 during preliminary experiments.

References

Azioune A, Storch M, Bornens M, Théry M, Piel M. 2009. Simple and rapid process for single cell micro-patterning. *Lab Chip* 9: 1640–1642.

Azioune A, Carpi N, Tseng Q, Théry M, Piel M. 2010. Protein micropatterns: A direct printing protocol using deep UVs. *Methods Cell Biol* 97:133–146.

Bartolini F, Gundersen GG. 2006. Generation of noncentrosomal microtubule arrays. *J Cell Sci* 119:4155–4163.

Bieling P, Telley IA, Surrey T. 2010. A minimal midzone protein module controls formation and length of antiparallel microtubule overlaps. *Cell* 142:420–432.

Braun M, Drummond DR, Cross RA, McAinsh AD. 2009. The kinesin-14 Klp2 organizes microtubules into parallel bundles by an ATP-dependent sorting mechanism. *Nat Cell Biol* 11:724–730.

Braun M, Lansky Z, Fink G, Ruhnnow F, Diez S, Janson ME. 2011. Adaptive braking by Ase1 prevents overlapping microtubules from sliding completely apart. *Nat Cell Biol* 13:1259–1264.

Carazo-Salas RE, Antony C, Nurse P. 2005. The kinesin Klp2 mediates polarization of interphase microtubules in fission yeast. *Science* 309:297–300.

Dinarina A, Pugieux C, Corral MM, Loose M, Spatz J, Karsenti E, Nedelec F. 2009. Chromatin shapes the mitotic spindle. *Cell* 138: 502–513.

Fache V, Gaillard J, Van Damme D, Geelen D, Neumann E, Stoppin-Mellet V, Vantard M. 2010. Arabidopsis kinetochore fiber-associated MAP65-4 cross-links microtubules and promotes microtubule bundle elongation. *Plant Cell* 22:3804–3815.

Fink G, Hajdo L, Skowronek KJ, Reuther C, Kasprzak AA, Diez S. 2009. The mitotic kinesin-14 Ncd drives directional microtubule-sliding. *Nat Cell Biol* 11:717–723.

Furuta K, Toyoshima YY. 2008. Minus-end-directed motor Ncd exhibits processive movement that is enhanced by microtubule bundling in vitro. *Curr Biol* 18:152–157.

Hackney DD, Jiang W. 2001. Assays for kinesin microtubule-stimulated ATPase activity. *Methods Mol Biol* 164:65–71.

Holy TE, Dogterom M, Yurke B, Leibler S. 1997. Assembly and positioning of microtubule asters in microfabricated chambers. *Proc Natl Acad Sci USA* 94:6228–6231.

Hyman A, Drechsel D, Kellogg D, Salser S, Sawin K, Steffen P, Wordeman L, Mitchison T. 1991. Preparation of modified tubulins. *Methods Enzymol* 196:478–485.

Janson ME, Loughlin R, Loïdouce I, Fu C, Brunner D, Nédélec FJ, Tran PT. 2007. Crosslinkers and motors organize dynamic microtubules to form stable bipolar arrays in fission yeast. *Cell* 128: 357–368.

Jiang K, Akhmanova A. 2011. Microtubule tip-interacting proteins: a view from both ends. *Curr Opin Cell Biol* 23:94–101.

Kapitein LC, Peterman EJG, Kwok BH. 2005. The bipolar mitotic kinesin Eg5 moves on both microtubules that it crosslinks. *Nature* 435:114–118.

Laan L, Pavin N, Husson J, Romet-Lemonne G, van Duijn M, López MP, Vale RD, Jülicher F, Reck-Peterson SL, Dogterom M. 2012. Cortical dynein controls microtubule dynamics to generate pulling forces that position microtubule asters. *Cell* 148:502–514.

Li H, Mao T, Zhang Z, Yuan M. 2007. The AtMAP65-1 cross-bridge between microtubules is formed by one dimer. *Plant Cell Physiol* 48:866–874.

Loïdouce I, Staub J, Setty TG, Nguyen NT, Paoletti A, Tran PT. 2005. Ase1p organizes antiparallel microtubule arrays during interphase and mitosis in fission yeast. *Mol Biol Cell* 16:1756–1768.

Loughlin R, Riggs B, Heald R. 2008. SnapShot: motor proteins in spindle assembly. *Cell* 134:548–548.e1.

Loughlin R, Wilbur JD, McNally FJ, Nedelec FJ, Heald R. 2011. Katanin contributes to interspecies spindle length scaling in *Xenopus*. *Cell* 147:1397–1407.

Malekzadeh-Hemmat K, Gendry P, Launay JF. 1993. Rat pancreas kinesin: identification and potential binding to microtubules. *Cell Mol Biol (Noisy-le-Grand)* 39:279–285.

Meng Q, Du J, Li J, Lü X, Zeng X, Yuan M, Mao T. 2010. Tobacco microtubule-associated protein, MAP65-1c, bundles and stabilizes microtubules. *Plant Mol Biol* 74:537–547.

Mimori-Kiyosue Y. 2011. Shaping microtubules into diverse patterns: molecular connections for setting up both ends. *Cytoskeleton (Hoboken)* 68:603–618.

- Nedelec F, Surrey T, Leibler S, Maggs AC. 1997. Self-organization of microtubules and motors. *Nature* 389:305–308.
- Reymann A-C, Martiel J-L, Cambier T, Blanchoin L, Boujemaa-Paterski R, Théry M. 2010. Nucleation geometry governs ordered actin networks structures. *Nat Mater* 9:827–832.
- Reymann A-C, Boujemaa-Paterski R, Martiel J-L, Guérin C, Cao W, Chin HF, De La Cruz EM, Théry M, Blanchoin L. 2012. Actin network architecture can determine myosin motor activity. *Science* 336:1310–1314.
- Sambrook J, Fritsch EF, Maniatis T. 1989. *Molecular Cloning: A Laboratory Manual*. Cold Spring Harbor, NY: Cold Spring Harbor Laboratory Press.
- Sasabe M, Machida Y. 2006. MAP65: a bridge linking a MAP kinase to microtubule turnover. *Curr Opin Plant Biol* 9:563–570.
- Shang W, Crone DE, Yang H, Dordick JS, Palazzo RE, Siegel RW. 2009. Using centrosome fragments in the directed assembly of microtubules. *J Nanosci Nanotechnol* 9:871–875.
- Sharp DJ, Rogers GC, Scholey JM. 2000. Microtubule motors in mitosis. *407:41–47*.
- Shelanski ML. 1973. Chemistry of the filaments and tubules of brain. *J Histochem Cytochem* 21:529–539.
- Subramanian R, Wilson-Kubalek EM, Arthur CP, Bick MJ, Campbell EA, Darst SA, Milligan RA, Kapoor TM. 2010. Insights into antiparallel microtubule crosslinking by PRC1, a conserved nonmotor microtubule binding protein. *Cell* 142:433–443.
- Surrey T, Nedelec F, Leibler S, Karsenti E. 2001. Physical properties determining self-organization of motors and microtubules. *Science* 292:1167–1171.
- Théry M. 2010. Micropatterning as a tool to decipher cell morphogenesis and functions. *J Cell Sci* 123:4201–4213.
- Tran PT, Marsh L, Doye V, Inoué S, Chang F. 2001. A mechanism for nuclear positioning in fission yeast based on microtubule pushing. *J Cell Biol* 153:397–411.
- Tulin A, McClerkin S, Huang Y, Dixit R. 2012. Single-molecule analysis of the microtubule cross-linking protein map65-1 reveals a molecular mechanism for contact-angle-dependent microtubule bundling. *Biophys J* 102:802–809.
- Van Damme D, Van Poucke K, Boutant E, Ritzenthaler C, Inzé D, Geelen D. 2004. In vivo dynamics and differential microtubule-binding activities of MAP65 proteins. *Plant Physiol* 136:3956–3967.
- Walczak CE, Shaw SL. 2010. A MAP for bundling microtubules. *Cell* 142:364–367.
- Walczak CE, Vernos I, Mitchison TJ, Karsenti E, Heald R. 1998. A model for the proposed roles of different microtubule-based motor proteins in establishing spindle bipolarity. *Curr Biol* 8:903–913.
- Walker RA, Brien O, Pryer K, Soboeiro ME, Voter WA, Erickson HP, Salmon ED. 1988. Dynamic instability of individual microtubules. *J Cell Biol* 107:1437–1448.
- Wordeman L. 2011. How kinesin motor proteins drive mitotic spindle function: lessons from molecular assays. *Semin Cell Dev Biol* 21:260–268.
- Yang Y, Deymier PA, Wang L, Guzman R, Hoying JB, McLaughlin HJ, Smith SD, Jongewaard IN. 2006. Nucleation and growth of microtubules from gamma-tubulin-functionalized gold surfaces. *Biotechnol Progr* 22:303–312.